


warm equatorial areas. However, it has been mentioned already a long time ago that different circulation regimes could have been present in the past, for example a salinity driven regime with heaviest water in the lower latitudes. In this section, potential mechanisms for both changes in mean state and for oscillatory behavior are discussed.

### 6.2.1. Advective feedback



Using a two-box model, as introduced in section 3.1, the possibility of multiple equilibria under similar surface forcing conditions was discovered (Stommel, 1961) about 40 years ago. Responsible for this non-uniqueness is a nonlinear feedback between the flow and the density structure, called the (salt) advection feedback. Consider in Fig. 6.4 a zonally averaged (overturning) circulation from the equator towards northern latitudes. The surface forcing saltens/warms the low latitude region and freshens/cool the high latitude region and the circulation is driven by the meridional density gradient. Since there is northern sinking, the circulation is thermally driven. If the circulation strengthens, then more salt is transported northward. This enhanced salt transport will increase the density in the north and consequently amplify the original perturbation in the circulation. The strengthening of the circulation also transports more heat northward, which will weaken the flow by lowering the density. Heat transport therefore provides a negative feedback on the circulation.

In addition to the advection feedback, a central ingredient to the existence of multiple steady states are the different damping times of salinity and temperature anomalies. The atmosphere exerts quite a strong control on the sea surface temperature anomalies, but salinity in the ocean does not affect the freshwater flux at all. In the two-box model in section 3.1, these different response time scales of salinity and temperature, with  $\tau_S = 1/R_S$  and  $\tau_T = 1/R_T$ , were taken into account by the coefficient  $\eta_3 = R_S/R_T = \tau_T/\tau_S$ , which was smaller than unity. In general, the different surface boundary conditions for temperature and salinity are referred to as mixed boundary conditions (Haney, 1971; Welander, 1986; Tziperman et al., 1994). The extreme case is a prescribed surface temperature ( $\tau_T \ll 1$ ) and prescribed surface freshwater flux ( $\tau_S \gg 1$ ) for which surface temperature perturbations are essentially zero. As seen in chapter 3, multiple equilibria arise if indeed the ratio  $\eta_3 < 1$  and only under certain forcing conditions (Fig. 3.4), i.e. a particular area in the  $(\eta_1, \eta_2)$  plane.

Together, the advective feedback and the different response time scales provide a potential mechanism of change of the thermohaline circulation. Consider again the thermally driven circulation as in Fig. 6.4 and imagine that a surface freshwater anomaly is suddenly present in the north part of the domain. Because the density is lowered in the north, the meridional buoyancy gradient decreases and hence the strength of the circulation decreases. The effect is that both the northward salt and heat transport decrease. Now, the negative heat anomaly is rapidly damped

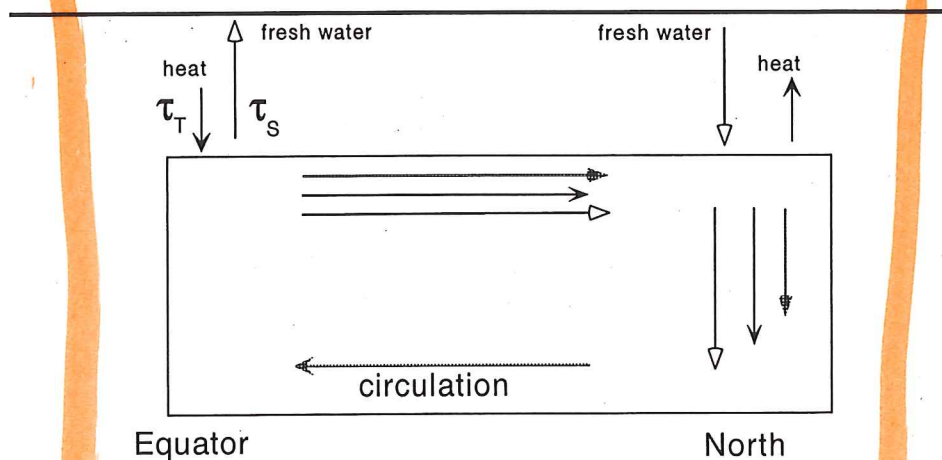


Figure 6.4. Sketch of the physics of the salt advection feedback. The mean circulation is indicated by the closed arrows. The upper ocean temperature and salinity fields can be inferred from the surface forcing of heat and freshwater. A perturbation which strengthens the circulation leads to a northward salt transport, which leads to amplification (open arrows) of the circulation (positive feedback). The perturbation in the circulation also leads to increased heat transport which opposes (negative feedback) the original perturbation (closed arrows).

at the sea surface, but the freshwater anomaly is not damped at all and hence amplifies the original freshwater perturbation. This positive feedback is able to rapidly weaken the thermally driven overturning circulation.

### 6.2.2. Convective feedback

A convective feedback may also be responsible for multiple equilibria (Welander, 1982; Lenderink and Haarsma, 1994). Consider in Fig. 6.5 a box model with time-varying temperature  $T_*$  and salinity  $S_*$  due to a surface heat fluxes  $F_T = \alpha(T_a - T_*)$  and surface salinity flux  $F_S$  in the surface box, coupled to a box with constant temperature  $T_i$  and  $S_i$  and constant prescribed flow rate  $q$ . Convective exchange with time constant  $\tau^{-1}$  occurs if the surface water becomes denser than the deep water, which has constant temperature  $T_b$  and salinity  $S_b$ . For  $q = 0$ , the model reduces to the model used by Welander (1982), and when there is no vertical exchange, the model can be considered as a limit of the Stommel (1961) model, for which the surface forcing in the equatorial box is adjusted such that temperature and salinity  $T_i$  and  $S_i$  remain constant.

The equations for the evolution of the temperature  $T_*$  and  $S_*$  are

$$\frac{dT_*}{dt_*} = \alpha(T_a - T_*) + q(T_i - T_*) + \tau_c \mathcal{H}(\rho_* - \rho_b)(T_b - T_*) \quad (6.1a)$$

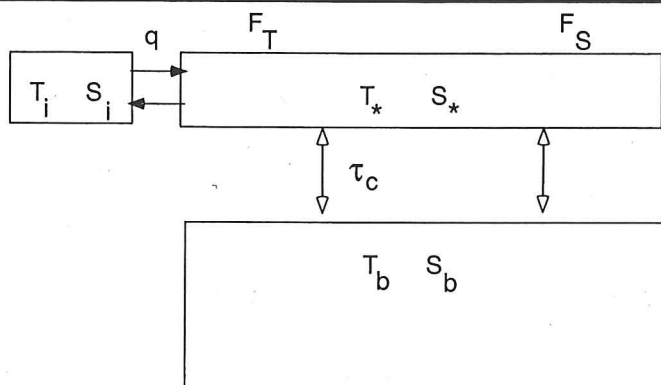


Figure 6.5. Sketch of the box model set-up to illustrate the convective feedback. An active box of temperature  $T_*$ ,  $S_*$  is coupled to boxes of constant temperature  $T_i$ ,  $S_i$  and  $T_b$ ,  $S_b$ . Advective exchange takes place with flow rate  $q$  and vertical (convective) exchange occurs, on a time scale  $\tau_c$ , if the surface water is denser than the bottom water.

$$\frac{dS_*}{dt_*} = F_S + q(S_i - S_*) + \tau_c \mathcal{H}(\rho_* - \rho_b)(S_b - S_*) \quad (6.1b)$$

with  $\mathcal{H}$  being the Heaviside function. With the equation of state

$$\rho_*(T_*, S_*) = \rho_0 - \alpha_T T_* + \alpha_S S_* \quad (6.2)$$

the steady states can be easily solved and become

$$T_* = \frac{qT_i + \alpha T_a + \tau_c \mathcal{H}(\rho_* - \rho_b)T_b}{q + \alpha + \tau_c \mathcal{H}(\rho_* - \rho_b)} \quad (6.3a)$$

$$S_* = \frac{qS_i + F_S + \tau_c \mathcal{H}(\rho_* - \rho_b)S_b}{q + \tau_c \mathcal{H}(\rho_* - \rho_b)} \quad (6.3b)$$

Two types of equilibria can be distinguished. Those for which the argument of the Heaviside function is positive are called convective equilibria, and those for which it is negative are called non-convective equilibria. With the new parameters

$$\Phi_T = -\alpha_T(\alpha(T_a - T_b) + q(T_i - T_b)) \quad (6.4a)$$

$$\Phi_S = \alpha_S(F_S + q(S_i - S_b)) \quad (6.4b)$$

$$\kappa(\tau_c) = \frac{q + \tau_c}{q + \tau_c + \alpha} \quad (6.4c)$$

three different solution regimes exist (Fig. 6.6).

The condition that a convective equilibrium exists can be written as  $\Phi_S > -\kappa(\tau_c)\Phi_T$  (indicated as the line  $a - b$  in Fig. 6.6) which defines regime 1 in

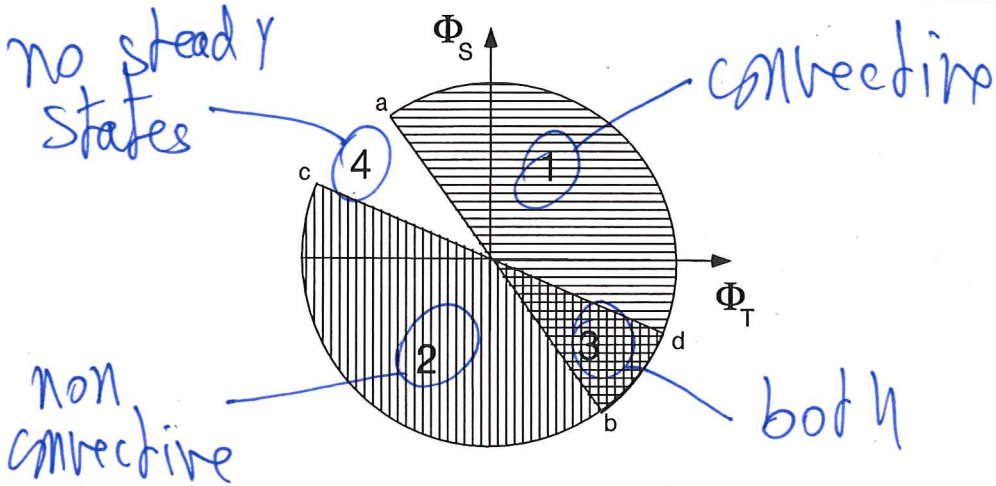


Figure 6.6. Sketch of the regimes of convective and non-convective equilibria in the box model in the  $(\Phi_T, \Phi_S)$  parameter plane. In regime 1, there are convective states, in regime 2 there are non-convective states, whereas in regime 3 both states are present. In regime 4 no steady states exist.

Fig. 6.6. Similarly, the condition for a non-convective equilibrium to exist can be written as  $\Phi_S < -\kappa(0)\Phi_T$  (indicated as the line  $c - d$  in Fig. 6.6) which defines regime 2. In regime 3, both convective and non-convective equilibria exist and transitions between these solutions can occur under the same forcing conditions. Consider a non-convective state with cold/freshwater above warm/salty water which is only marginally stable and an atmospheric forcing which is cooling and freshening the upper box. A finite amplitude positive density perturbation is able to induce convection and if this occurs, warmer and saltier water is mixed to the surface. The heat in the surface layer is quickly lost to the atmosphere but the surface salinity is increased and hence convection is maintained, leading to a convective state.

For the particular case  $\Phi_T = 1.0$ ,  $q/\alpha = 0.5$  and  $\tau/\alpha = 2.0$ , the bifurcation diagram of the model (6.1) is plotted. In this diagram, both the dimensionless temperature  $T = \alpha_T(T_* - T_b)$  and salinity  $S = \alpha_S(S_* - S_b)$  are plotted versus the control parameter  $\Phi_S$ . Two saddle node bifurcations ( $L_1$  and  $L_2$ ) occur at  $\Phi_S = -5/7$  and  $\Phi_S = -1/3$ . These are exactly the values  $-\kappa(\tau)$  and  $-\kappa(0)$  bounding the regions of convective and non-convective regimes, respectively. Hence, the high temperature and salinity states are convective and exist for  $\Phi_S > -5/7$  (regime 1) whereas the low salinity and temperature states are non-convective and exist for  $\Phi_S < -1/3$  (regime 2). Regime 3 is exactly located in the interval  $-5/7 < \Phi_S < -1/3$  and in this regime, multiple equilibria exist. Note that

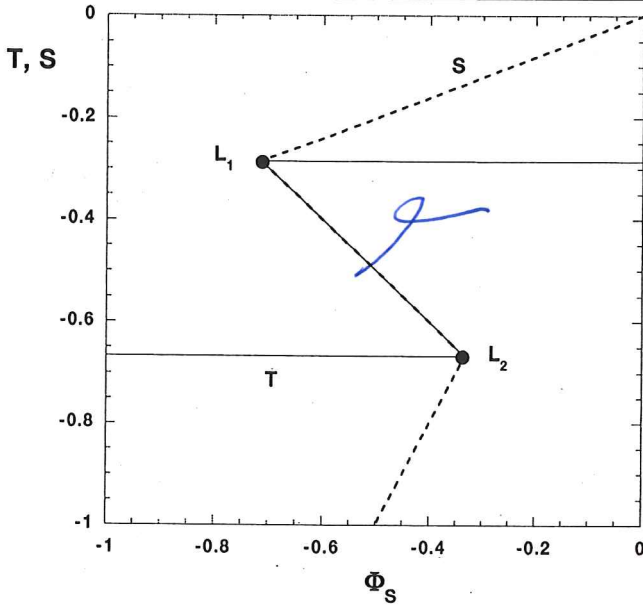


Figure 6.7. Bifurcation diagram for the box model (6.1) with  $\Phi_T = 1.0$ ,  $q/\alpha = 0.5$  and  $\tau/\alpha = 2.0$  and  $\Phi_S$  as control parameter.

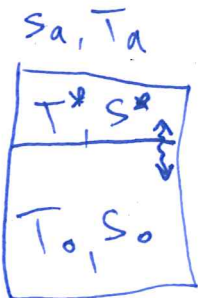
regime 4 is not reached here, because  $\Phi_T > 0$ .

### 6.2.3. The flip-flop oscillation

Within simple box models, two types of oscillatory phenomena can be found. One is associated with propagation of perturbations along the mean thermohaline flow which will be subject of the next subsection and another is associated with transitions between convective and non-convective states. This type of oscillation was found by Welander (1982) in a box model which is a special case of the model in section 6.2.2. Only two boxes which exchange heat and salt vertically are considered and moreover the ocean-atmosphere salinity flux is chosen as  $F_S = \beta(S_a - S_*)$ , with different restoring times for freshwater and heat. With  $q = 0; T_b = T_0; S_b = S_0; \rho_b = \rho_0$  in (6.1) and with a more general form of the convective exchange function  $k(\rho_*, \rho_0)$  the model equations become

$$\frac{dT_*}{dt_*} = \alpha(T_a - T_*) + k(\rho_*, \rho_0)(T_0 - T_*) \tag{6.5a}$$

$$\frac{dS_*}{dt_*} = \beta(S_a - S_*) + k(\rho_*, \rho_0)(S_0 - S_*) \tag{6.5b}$$



with the equation of state (6.2).

One of the cases considered (Welander, 1982) is  $T_0 = S_0 = 0$  and

$$\begin{aligned} k(\rho_*) &= 0, \rho_* \leq \varepsilon \\ k(\rho_*) &= k, \rho_* \geq \varepsilon \end{aligned}$$

which means that if the surface density  $\rho_*$  becomes slightly larger than the density in the bottom box, an exchange flux ( $-kT_*$ ) is generated for both temperature and salinity with constant exchange coefficient  $k$ .

For the particular choice of parameters

$$\frac{\alpha_T T_a}{\alpha_S S_a} = 0.2; \quad \frac{\alpha}{\beta} = 10; \quad \frac{k}{\alpha} = 5; \quad \frac{\varepsilon}{\alpha_S S_a} = -0.01 \quad (6.6)$$

a trajectory is plotted in Fig. 6.8a. All fields oscillate and the oscillation seems to be sustained. In Welander (1982), it is shown that it damps for the case  $\varepsilon = 0.0$ , hence a nonzero  $\varepsilon$  is essential to the existence of the oscillation.

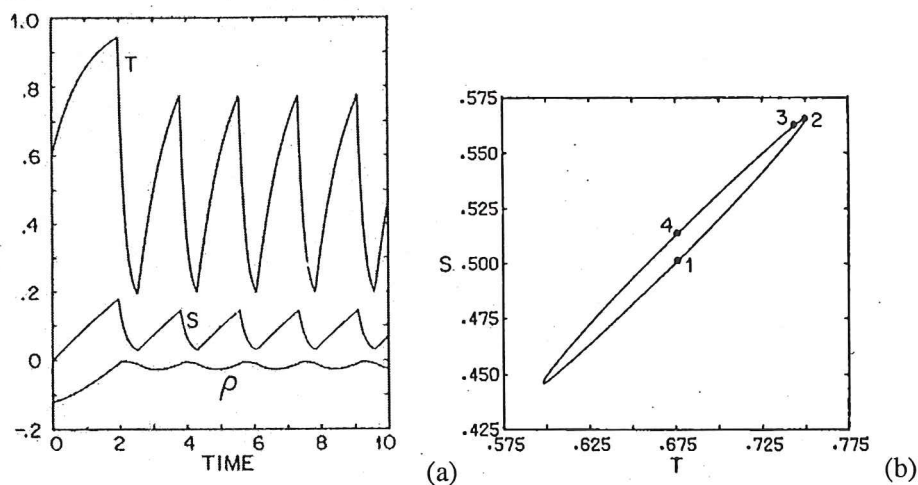


Figure 6.8. (a) Trajectory of the box model (6.5) for  $\varepsilon \neq 0$  in the convective exchange function (6.5) showing the oscillation in temperature  $T = T_*/T_a$ , salinity  $S = S_*/S_a$  and density  $\rho = \rho_*/\rho_a$ . (b) Phase plane picture of the oscillation in (a), where  $T_*/T_a$  is plotted versus  $S_*/S_a$  (Welander, 1982).

The advantage of these type of models is that the oscillation can be understood in quite detail. In the particular case above, the model has two steady states. The non-convective state is given by

$$\bar{\rho}_* \leq \varepsilon; \quad \bar{T}_* = T_a; \quad \bar{S}_* = S_a \quad (6.7)$$

and the convective state by

$$\bar{\rho}_* > \varepsilon : \bar{T}_* = \frac{\alpha T_a}{\alpha + k} \quad (6.8a)$$

$$\bar{S}_* = \frac{\beta S_a}{\beta + k} \quad (6.8b)$$

with

$$\bar{\rho}_* = -\alpha_T \bar{T}_* + \alpha_S \bar{S}_*$$

There exists a parameter regime (similar to regime 4 in Fig. 6.6), where both steady states cannot be reached. The trajectory then oscillates between both steady states without actually reaching them. A phase-plane picture of the oscillation in Fig. 6.8a is plotted in Fig. 6.8b. At point 1,  $T$  and  $S$  are such that  $\rho_* < \varepsilon$  so that the trajectory is attracted towards the non-convective steady state and both  $T$  and  $S$  increase (towards point 2). This steady state is never reached, because at point 3, the boundary  $\rho_* = \varepsilon$  is crossed and convection occurs. Then the trajectory is attracted towards the convective steady state, but it also does not reach this state because at some point, convection will stop. Hence, the oscillation can be described as a 'flip-flop' between convective and non-convective states, where during the oscillation neither of these states is actually reached.

#### 6.2.4. The loop oscillation

The most elementary box model which includes a loop oscillation is the four-box model originally used by Huang et al. (1992) and analysed in more detail in Tziperman et al. (1994). It differs from the two-box model by including two deep boxes and vertical exchange of heat and salt (Fig. 6.9a). The surface and deep boxes may have different volumes, but their ratio is fixed and Tziperman et al. (1994) mostly consider the case of equal volumes. The surface boundary conditions consist of fresh-water fluxes  $H_1$  and  $H_2$ , atmospheric temperatures  $T_1^a$  and  $T_2^a$  and the transport  $q_*$  is related to the average north-south density difference. The governing equations of this box model can be found in Tziperman et al. (1994), where also values of the parameters are provided.

A typical bifurcation diagram of this model is plotted in Fig. 6.9b with the (dimensionless) freshwater flux  $E - P = H_1 + H_2$  as control parameter. On the vertical axis, the buoyancy ratio is plotted with  $\Delta T = T_{1*} - T_{2*}$  and  $\Delta S = S_{1*} - S_{2*}$ . The basic thermally driven state is stable for small  $E - P$ , but it loses stability due to a Hopf bifurcation (the point marking the transition between '\*' and 'o' in Fig. 6.9b at  $E - P \approx 110$ ). The pair of complex conjugated eigenvalues which have crossed the imaginary axis become real for slightly larger values of  $E - P$  (at the transition of 'o' and 'x') and then one of them moves into the left complex plane at the saddle node bifurcation (at  $E - P \approx 125$ ) and a branch of unstable solutions exists at smaller values of  $E - P$ . The mechanism of the oscillatory

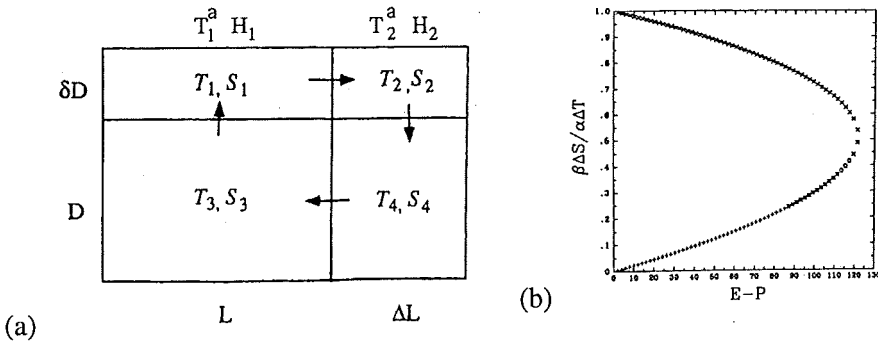


Figure 6.9. (a) Sketch of the box model to illustrate the loop oscillation (Tziperman et al., 1994). (b) Bifurcation diagram for the 4-box model in (a) as used in Tziperman et al. (1994). The markers correspond to the stability of the flow: '+' indicates stability, '\*' indicates stability but the least stable mode is oscillatory, 'o' corresponds to an oscillatory instability and 'x' to instability.

instability was investigated in Tziperman et al. (1994) and shown to be related to the propagation of a salinity anomaly along the mean flow. This mechanism is very similar to that of the Howard-Malkus loop oscillation discussed in Welander (1986). It will be considered in more detail in the context of a somewhat more complex model below (section 6.4.3).

### 6.2.5. Models of the thermohaline circulation

Certainly box models are useful to illustrate basic physical phenomena, but more complex models are needed to capture the full spatial-temporal behavior of the thermohaline circulation. Contrary to the wind-driven circulation in the previous chapter, now also the modelling of the heat and salt transport is essential. Starting point of all the models are the full (Boussinesq) primitive equations, with velocity vector  $\mathbf{v}_*$  and pressure  $p_*$ , which were presented in chapter 2 but repeated here for convenience.

$$\rho_0 \left[ \frac{D\mathbf{v}_*}{dt_*} + 2\Omega \wedge \mathbf{v}_* \right] = -\nabla p_* - g\rho_* \mathbf{e}_3 + \rho_0 \mathcal{F}_{I*} \quad (6.9a)$$

$$\nabla \cdot \mathbf{v}_* = 0 \quad (6.9b)$$

$$\rho_0 C_p \frac{DT_*}{dt_*} = \mathcal{F}_{T*} \quad (6.9c)$$

$$\rho_0 \frac{DS_*}{dt_*} = \mathcal{F}_{S*} \quad (6.9d)$$

$$\rho_* = \rho_0(1 - \alpha_T(T_* - T_0) + \alpha_S(S_* - S_0)) \quad (6.9e)$$